Environmental Science & Technology

pubs.acs.org/est

Article

Physical Contact between Bacteria and Carbonaceous Materials: The Key Switch Triggering Activated Carbon and Biochar to Promote Microbial Iron Reduction

Lin Shen, Xiao Zhu, Haoze Jiang, Juntao Zhang, Chengyu Chen, John R. Reinfelder, Andreas Kappler, Liping Fang, Tongxu Liu, Chuanping Liu, Yundang Wu,* and Fangbai Li

Cite This: *Environ. Sci. Technol.* 2025, 59, 9576−9586

Read Online

ACCESS | Metrics & More | Article Recommendations | Supporting Information

ABSTRACT: Carbonaceous materials, including activated carbon and pyrolytic carbon, have been recognized for about over a decade as effective electron shuttles or conductive materials in promoting microbial Fe(III) mineral reduction. However, recent studies reveal inhibitory effects, sparking debates about their overall impact. We hypothesized that the physical contact between bacteria and carbon is an overlooked yet critical factor in determining whether carbon promotes or inhibits microbial Fe(III) reduction. Using systems containing *Shewanella oneidensis* MR-1, activated carbon, and ferrihydrite, we investigated how carbon−iron oxide aggregate structure affects Fe(III) reduction kinetics. At low activated carbon-to-iron oxide ratios (C/Fe = 5:7 by mass), ferrihydrite aggregated with carbon, forming carbon-encapsulated particles that suppressed Fe(III) reduction rates. Conversely, at higher ratios (C/Fe = 100:7), the ferrihydrite dispersed on the carbon surface, enhancing both the rate and extent of Fe(III) reduction. Tests with 11 different carbonaceous materials (activated carbon and biochar) all confirmed that the microstructure of iron oxides—whether encapsulating or dispersed—on carbon surfaces is critical for determining Fe(III) reduction rates. This insight resolves the debate on whether carbonaceous materials promote or inhibit Fe(III) mineral reduction and enhances our understanding of their roles in biogeochemical processes and environmental remediation.

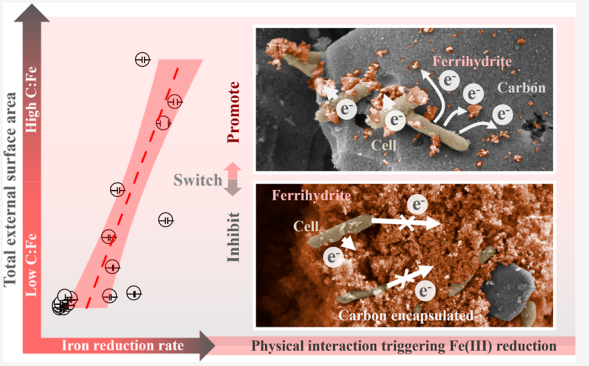

KEYWORDS: *Fe(III) reduction, activated carbon, pyrolytic carbon, aggregate structure, extracellular electron transfer*

INTRODUCTION

Carbonaceous materials, including activated carbon and biochar, are widely used as soil amendments to reduce the effects of soil acidification and chemical contamination.[1−7] In addition to their traditionally recognized capacity to adsorb heavy metals[8,9] and regulate pH,[1,10,11] carbonaceous materials can also mediate electron transfer between microorganisms and iron(III) (oxyhydr)oxide minerals, which for simplicity we refer to as iron oxides.[12,13] These carbonaceous materials are capable of electron shuttling,[14−16] the release of dissolved organic matter (DOM),[17−19] and increasing bulk conductivity,[20,21] thereby accelerating microbial Fe(III) reduction.[22] Whether serving as an electron shuttle or a conductive material, the physical interactions between microorganisms, the carbon material, and iron oxides are essential for the reaction to occur.[23,24] However, many studies overlooked the importance of the adsorption of cells and iron on the surfaces of carbonaceous materials in these multiphase reactions, making the microstructure of carbon−iron oxide aggregates a critical yet underexplored factor in understanding the role of carbonaceous materials in microbial Fe(III) reduction.

The aggregation of iron oxides and carbon particles is controlled by electrostatic forces and other physical and chemical effects. Typically, biochar carries a negative charge, while iron oxides such as ferrihydrite, goethite, and hematite are positively charged.[25] The positively charged Fe−OH groups on the surface of iron oxides tend to electrostatically adsorb onto the negatively charged COOH and C═O groups on the surface of carbon materials.[26] van der Waals forces may also facilitate the adsorption and aggregation of iron and carbon particles.[27] In the environment, the aggregation of biochar and iron oxides is influenced by pH, ionic strength, and the concentration of humic acids, as well as particle size.[25,28,29] How natural variation in the structure of iron oxide−carbon aggregates affects microbial iron reduction in

Received: December 13, 2024
Revised: April 2, 2025
Accepted: April 3, 2025
Published: April 10, 2025

particular and iron−carbon−microbe interactions in general is not clearly understood.

Although the role of carbonaceous materials in promoting microbial Fe(III) mineral reduction has been widely recognized, recent studies have noted that their influence on interactions between microorganisms, carbon, and minerals can sometimes lower or even inhibit the rate of Fe(III) reduction. This is attributed to the effects caused by changes in physical interactions. It has been observed that biochar can adsorb bacterial cells, thereby reducing the interaction between the cells and ferrihydrite.[30] A similar phenomenon was observed in research on nontronite reduction.[31] In these studies, biochar inhibited microbial Fe(III) reduction by minimizing physical contact between cells and the iron oxides. However, due to the negative zeta potential of carbonaceous materials such as activated carbon and biochar in most environments,[32−36] along with the positive zeta potential of poorly crystalline iron oxides (pH < 8.2),[37,38] carbonaceous materials are more likely to adsorb iron oxides than microbes. In prior studies on ferrihydrite, researchers used optical and fluorescence microscopy to observe iron−carbon−microbe interactions.[30] While these methods clearly showed microbial spatial positioning, they provided limited insight into the physical interactions between carbon and iron oxides. Moreover, these studies did not quantify the physical aggregation between iron and carbon. Additionally, carbonaceous materials interact with both minerals and microorganisms and may also adsorb newly generated Fe(II).[39] As Fe(II) is key to catalyzing iron oxide transformations,[40,41] carbonaceous material adsorption may affect these processes. Considering the importance of the physical contact between cells, carbon and iron oxides, and the conflicting findings—some indicating promotion, others inhibition of Fe(III) reduction by carbonaceous materials—we hypothesized that the microstructure of carbon−iron oxide aggregates may be an important factor controlling this process.

Activated carbon is highly conductive[21,42] and also has active hydroxyl and carbonyl functional groups.[43] Compared to biochar, activated carbon is a more widely used adsorbent.[44] Therefore, to examine how the microstructure of carbon−iron oxides affects Fe(III) reduction, we selected two activated carbon compounds as representative materials for a systematic study and later used 9 different biochars from various sources prepared at different temperatures to verify the general principles. These carbonaceous materials were incorporated into a reaction system that included the Fe(III)-reducing bacterium *Shewanella oneidensis* MR-1[45] and poorly crystalline ferrihydrite.[46] The kinetics and extent of Fe(III) reduction, as well as the physical contact, were systematically studied. By varying the proportions of carbon, microorganisms, and iron, this study aims to test the hypothesis that the physical form of ferrihydrite on the surface of carbonaceous materials is the key factor that controls whether microbial Fe(III) reduction is inhibited or promoted. We hoped to clarify the ongoing debate about whether carbonaceous materials promote or inhibit microbial Fe(III) reduction, which will advance our understanding of the environmental effects of carbonaceous materials and their role in biogeochemical processes involving iron oxides.

MATERIALS AND METHODS

Materials Preparation. The microbial strain used in this experiment is *S. oneidensis* MR-1 (MR-1), a model organism for Fe(III)-reducing bacteria, purchased from the Microbial Culture Collection Center of the Chinese Academy of Agricultural Sciences (MCCC). PEC-02 (PEC) and YP-80F (YP) are coconut shell-based activated carbon materials obtained from Foshan Porous Carbon Tech Co., Ltd. PEC (1000 °C) and YP (1000 °C) refer to activated carbon pyrolyzed at 1000 °C in nitrogen for 2 h (heating rate: 5 °C/min) to remove oxygen-containing functional groups from their surfaces. The main difference between the two lies in their specific surface areas: YP has a surface area of 2277 m^2/g, while PEC has a surface area of 1885 m^2/g. For the description of all other chemical materials, including the selection of biochars and ferrihydrite synthesis,[46] please refer to Text S1.

Construction of the Fe(III) Reduction System. Fe(III)-reducing incubations were established using *S. oneidensis* MR-1 (OD_{600} = 0.5 or 1.0) with activated carbon or biochar, 10 mM lactate, 5 mM ferrihydrite, and 10 mM piperazine-*N*,*N*′-bis(2-ethanesulfonic acid) (PIPES) buffer (pH 7.0). Activated carbon concentrations were adjusted to achieve C/Fe ratios (g C/g Fe) of 5:7, 10:7, 25:7, and 100:7 to study carbon−iron interactions. For biochar, with a lower specific surface area, higher C/Fe ratios (12.5:7 and 250:7) were used. Log-phase MR-1 cells were washed with PIPES buffer to remove metabolites, resuspended, and transferred to serum bottles. After deoxygenation, serum bottles were sealed and incubated at 30 °C in the dark on a shaker at 200 rpm.

Chemical Characterization. Dissolved Fe(II) was measured via the *o*-phenanthroline colorimetric method after filtering the Fe(III)-reducing system solution through a 0.22 μm membrane in an anoxic chamber. HCl-extracted Fe(II), which includes the sum of dissolved and solid-phase Fe(II), was obtained by dissolving solid iron oxides in 1 M HCl (1:1 ratio with the sample) for 48 h, followed by filtration and analysis. Fe(II) was detected using a Full Wavelength Microplate Reader (Multiskan Sky, Thermo Scientific, USA). The concentration of Fe(II) extracted by HCl has been converted according to the sampling volume and dilution multiple. It has been converted back to the total Fe(II) concentration per milliliter of solution in the reactor, representing the total concentration of Fe(II) generated in the experimental vial. Fe(III) reduction kinetics were modeled with the Box−Lucas equation: $y = a \times (1 - e^{-bx})$, where a is the total Fe(II) production, b is the rate constant, and x is the time (hours). In the X-ray diffraction (XRD) analysis, samples from the iron-reducing system were collected and dried in a vacuum freeze-dryer (LGJ-25D, Beijing SiHuan Qihang Technology Co., Ltd., China) for about 3 days until powdered. The dried mineral precipitates were then ground and spread evenly on the X-ray diffractometer stage (Rigaku SmartLab SE, Rigaku Corporation, Japan). The test used a Cu target (λ = 1.5406 Å) with a scanning range of 2θ = 10−90° at a speed of 1°/min. The data were processed using MDI Jade 6 software and compared with mineral PDF cards to identify the crystalline phases. Other chemical analyses, including conductivity, specific surface area, particle size, zeta potential, functional groups, leachate dissolved organic carbon (DOC)[17,47] concentration, cyclic voltammetry, etc., are provided in Table S1.

Bioelectrochemical Analysis. In the elucidation of three different types of electron transfer mechanisms (solid-phase electron shuttling, leachate release, and electron transfer via conductivity), bioelectrochemical methods were used to provide supplementary evidence. We established an electrochemical system to assess PEC and YP's ability to facilitate

https://doi.org/10.1021/acs.est.4c14024
Environ. Sci. Technol. 2025, 59, 9576−9586

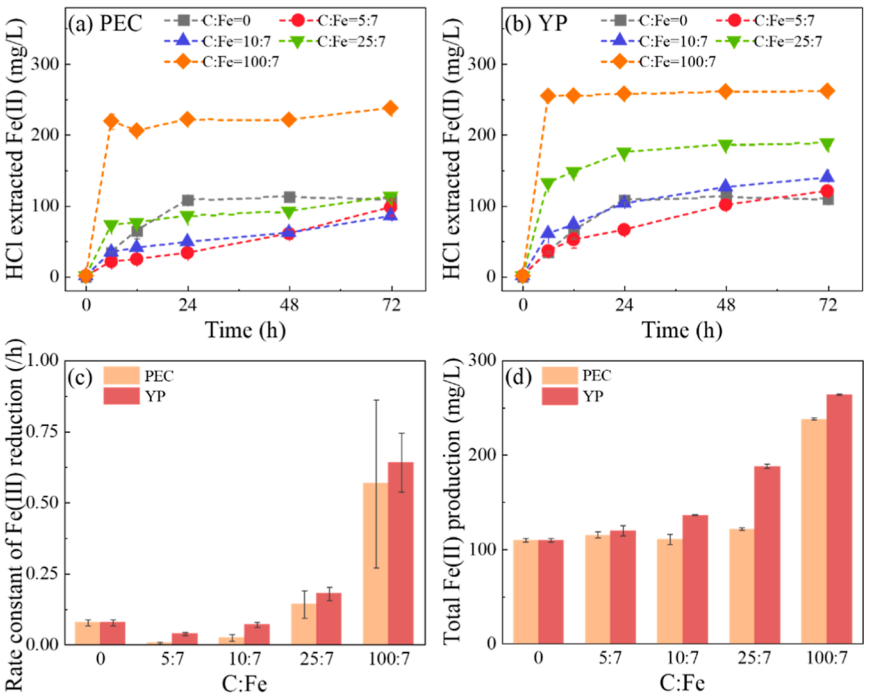

Figure 1. Microbial Fe(III) mineral reduction kinetics (with *Shewanella oneidensis* MR-1) in incubations with 5 mM ferrihydrite and increasing amounts of activated carbon materials (PEC or YP) to achieve a range of carbon-to-iron mass ratios (g C/g Fe). Results are the kinetics of Fe(II) production with (a) PEC and (b) YP, (c) Fe(III) mineral reduction rate constants (/h) and (d) total Fe(II) production over 72 h for both activated carbon materials at various carbon-to-iron ratios. The concentration of Fe(II) extracted by HCl has been converted according to the sampling volume and dilution multiple. It has been converted back to the total Fe(II) concentration per milliliter of solution in the reactor, representing the total concentration of Fe(II) generated in the experimental vial.

extracellular electron transfer from microorganisms to an electrode through their conductivity. The setup included MR-1 (OD_{600} = 2.0), 10 mM sodium lactate, 10 mM PIPES buffer (pH 7.0), and electrodes (platinum counter, calomel reference, glassy carbon working electrode coated with PEC or YP). Experiments were conducted at +0.2 V (vs SCE) and 30 °C under nitrogen protection, measuring current variations.

Morphology Analysis by Scanning Electron Microscope. The analysis aimed to observe the spatial relationships among ferrihydrite, microorganisms, and carbonaceous materials. Liquid samples from the Fe(III)-reducing system were centrifuged, and precipitates were fixed in 2.5% glutaraldehyde overnight at 4 °C, then washed with phosphate buffer. Samples were dehydrated in ethanol (30%, 50%, 70%, 90%, and 100%) and treated with *tert*-butanol before freeze-drying. Carbonaceous materials were adhered to conductive glue and gold-coated. The morphology and EDS mapping were captured using scanning electron microscope (SEM) (ZEISS GeminiSEM 300 and ProX, Phenom, Netherlands) at 3 kV for imaging and 15 kV for EDS.

RESULTS AND DISCUSSION

Impact of Activated Carbon on Microbial Fe(III) Reduction. The kinetics of microbial Fe(III) mineral reduction in incubations with various activated carbon-to-iron ratios were determined. Figure 1 illustrates that both the rate and total amount of microbial ferrihydrite reduction were influenced by carbon dosage.

First, iron reduction rate has changed. Addition of the lowest concentrations of activated carbon resulted in a decrease in Fe(III) reduction rates relative to incubations without activated carbon, but when the C/Fe ratio exceeded 25:7 for PEC or 10:7 for YP, Fe(III) reduction rates increased (Figure 1a,b). Thus, in incubations with a C/Fe ratio of 5:7, the rate constant of ferrihydrite reduction decreased from 0.077/h in the absence of activated carbon to 0.0058/h and 0.023/h with added PEC and YP, respectively (Figure 1c). However, with the highest amounts of activated carbon (C/Fe ratio of 100:7), rate constants of ferrihydrite reduction increased to 0.57/h and 0.64/h, for PEC and YP, respectively. The decrease in Fe(III) reduction was especially pronounced at low concentrations of PEC. Specifically, in the PEC incubations with C/Fe ratios of 5:7 and 10:7, the Fe(III) reduction rate constant decreased by factors of 12 and 2.2, respectively, compared to incubations with no added activated carbon. This suggests that lower concentrations of activated carbon inhibit microbial Fe(III) mineral reduction. These trends align with previous studies of biochar in which lower carbon concentrations tended to suppress Fe(III) mineral reduction, while higher concentrations enhanced the process.[30,31,48]

Second, the total reduction of Fe(III) has changed. Total Fe(II) production over 72 h in low activated carbon-to-iron ratio (5:7 and 10:7) incubations was not significantly different from that in incubations without added activated carbon, whereas the production of Fe(II) increased in incubations with high activated carbon-to-iron ratios (25:7 and 100:7) (Figure 1d). The total Fe(II) production increased from 109 mg/L in the absence of activated carbon to 237 and 262 mg/L with the highest amount of activated carbon. Activated carbon therefore influenced both the rate of Fe(III) reduction and the total amount Fe(II) produced. To investigate whether the total ferrihydrite reduction was limited by the number of Fe(III)-reducing bacteria, we conducted an experiment maintaining the activated carbon-to-iron ratio at 25:7 while doubling the

https://doi.org/10.1021/acs.est.4c14024
Environ. Sci. Technol. 2025, 59, 9576−9586

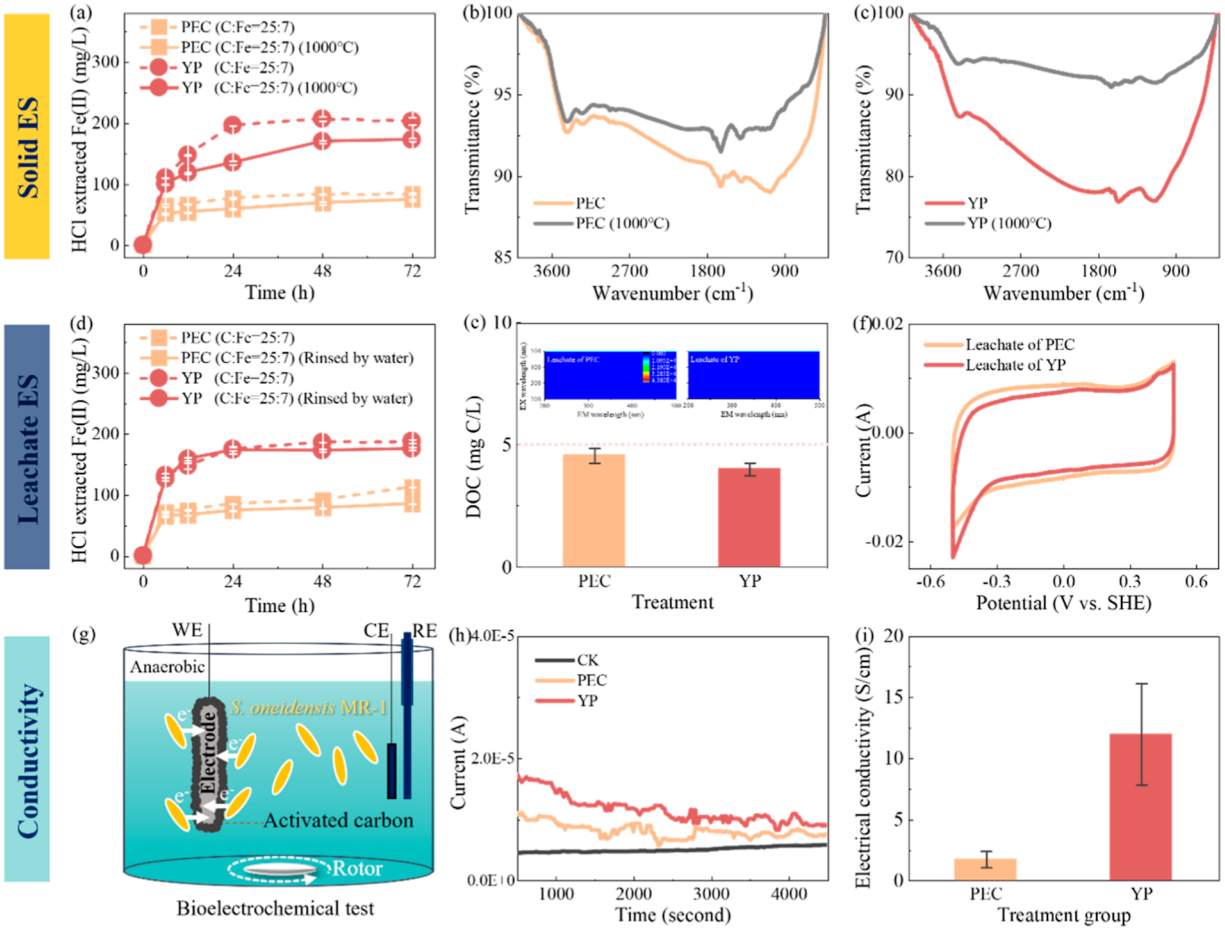

Figure 2. (a) Fe(III) reduction kinetics in incubations of ferrihydrite and *Shewanella oneidensis* MR-1 with PEC and YP before and after 1000 °C pyrolysis; (b,c) FTIR spectra of YP and PEC before and after pyrolysis; (d) Fe(III) reduction kinetics before and after washing treatment; (e) DOC concentration and EEM of DOC leached from 4.0 g/L PEC or YP (C/Fe ratio 100:7); (f) cyclic voltammetry of YP and PEC leachates; (g) schematic of the bioelectrochemical test system, where activated carbon blocks direct contact between microorganisms and the electrode, with stirring for mass transfer and microbial contact; (h) bioelectric current in activated carbon-loaded and unloaded (CK) systems; (i) conductivity of YP and PEC. ES: electron shuttling.

microbial biomass. The results showed that the Fe(III) reduction remained largely unchanged (Figure S1), suggesting that the extent of ferrihydrite reduction is primarily influenced by the activated carbon-to-iron ratio rather than microbial biomass.

Carbon materials also affect mineral transformation through the adsorption of dissolved Fe(II), which decreases the formation of reported reactive Fe(III) intermediates[49−51] and inhibits the Fe(II)-catalyzed phase transition.[40,41] This effect is evident in our XRD and Fe(II) adsorption results (Figure S2, Text S2), which show that both YP and PEC slowed down the conversion rate of ferrihydrite to thermodynamically stable crystalline phases such as goethite, hematite, and magnetite.[52−54]

Mechanism by Which Activated Carbon Accelerates Electron Transfer. According to previous reports, pyrolyzed carbon promotes electron transfer and accelerates Fe(III) mineral reduction through three mechanisms. First, oxygen-containing functional groups on the carbon material's surface can act as solid-state electron shuttles, mediating electron transfer between microorganisms and minerals.[12,14,55,56] Second, the leachate of the carbon material contains DOC, and the oxygen-containing functional groups (such as carbonyl and hydroxyl groups) in the DOC are redox active, serving as dissolved shuttles to accelerate extracellular electron transfer by microorganisms.[57−60] Third, high-temperature pyrolyzed carbon has good electrical conductivity, facilitating electron transfer through direct conductivity.[20,61,62] To clarify the main pathways by which activated carbon promotes electron transfer, we studied these three mechanisms.

First, we examined the role of surface functional groups as solid electron shuttles in Fe(III) reduction. High temperatures can degrade these groups, reducing their contribution.[63] Therefore, we pyrolyzed activated carbon at 1000 °C under anoxic conditions and compared its ability to promote Fe(III) reduction before and after treatment (Figure 2a). Results show a 20% decrease in total Fe(III) reduction with YP and a 17% decrease with PEC after pyrolysis. FTIR analysis revealed significant reductions in carbonyl and hydroxyl peaks on YP (Figure 2c), while PEC showed less reduction (Figure 2b), aligning with observed changes in Fe(III) reduction. Although Fe(III) reduction decreased after pyrolysis, high concentrations of activated carbon (C/Fe = 100:7) still significantly enhanced Fe(III) reduction compared to controls (Figure S3). These findings suggest that surface functional groups contribute to electron transfer, but other factors may also play a role.

https://doi.org/10.1021/acs.est.4c14024
Environ. Sci. Technol. 2025, 59, 9576−9586

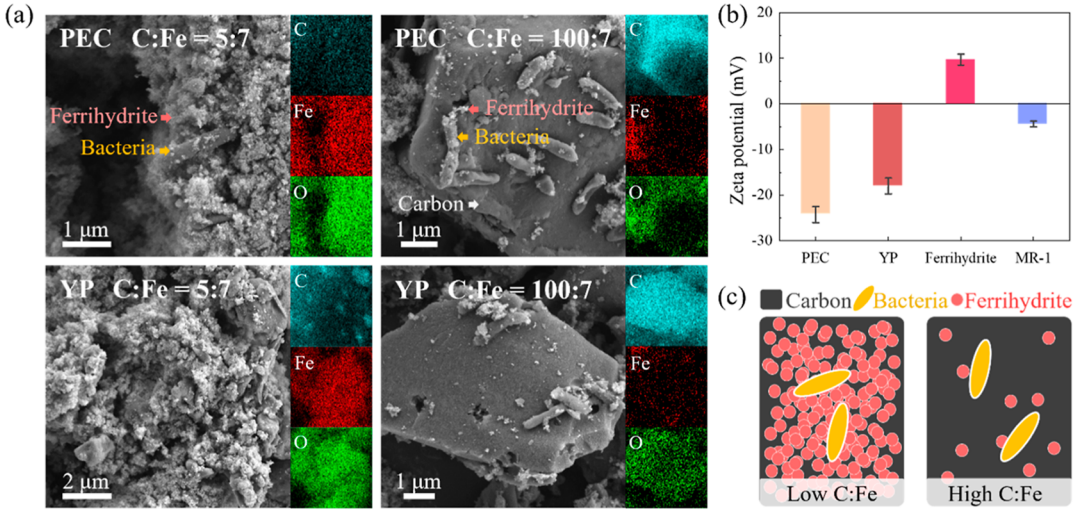

Figure 3. (a) SEM images showing physical contact between activated carbon, ferrihydrite, and microorganisms at low (5:7) and high (100:7) activated carbon-to-iron ratios; (b) zeta potentials of activated carbon, ferrihydrite, and bacterial cells; (c) schematic of physical contact between cells and activated carbon at low and high carbon-to-iron ratios. At low ratios, carbon is encapsulated by ferrihydrite; at high ratios, ferrihydrite disperses on the carbon surface, allowing direct cell contact.

Second, we examined the role of activated carbon leachate by comparing Fe(III) reduction rates before and after leachate removal. Results showed that removing the leachate had little impact on Fe(III) reduction ability (Figure 2d). YP's reduction decreased by only 4.3%. Although PEC's total Fe(III) reduction dropped by 19%, its reduction rate remained nearly identical (Figure S4). Excitation−emission matrix fluorescence (EEM) showed no fluorescence signals from DOC-like substances (Figure 2e), and cyclic voltammetry of the leachate revealed weak redox peaks (Figure 2f). The DOC concentration of the leachate was 4.0−4.2 mg C/L, below the effective electron shuttle concentration (>5 mg C/L).[64] These findings suggest that leachate has limited impact on electron transfer between microorganisms and iron oxides.

Finally, we constructed a bioelectrochemical system to evaluate the ability of activated carbon materials to mediate electron transfer through conductivity (Figure 2g). Applying a positive potential to the electrode simulated electron transfer between microorganisms, carbon, and iron oxides, with bioelectric current used as a measurement of conductivity. Since activated carbon separates the electrode from microorganisms, electron transfer depends mainly on the carbon's conductivity. In activated carbon-loaded systems, the current was slightly higher than that in unloaded systems, indicating that carbon's conductivity (Figure 2h) aids electron transfer. YP showed a stronger current than PEC (Figure 2h), consistent with their different conductivity (Figure 2i). The conductivities of YP (1.8 ± 0.67 S/cm) and PEC (12 ± 4.14 S/cm) were much higher than that of Fe(III)-reducing microbial nanowires (5 mS/cm),[65] sufficient to support microbial electron transfer.[42] This suggests that activated carbon mediates electron transfer effectively through its conductivity.

The above three mechanisms can explain the promotion of microbial Fe(III) reduction by carbon materials but cannot account for their inhibitory effects.

Microstructure of Activated Carbon−Ferrihydrite Aggregates. Physical contact among activated carbon, ferrihydrite, and microorganisms critically influenced electron transfer efficiency in our Fe(III)-reducing microcosms. Therefore, we conducted further investigation of the microstructure of activated carbon−ferrihydrite aggregates.

SEM observations of incubations with low (C/Fe = 5:7) and high (100:7) activated carbon-to-iron ratios revealed significant differences in the spatial relationships among iron, carbon, and microorganisms (Figure 3a). In the low activated carbon-to-iron ratio group (C/Fe = 5:7), ferrihydrite formed aggregates with activated carbon, simultaneously encasing some microorganisms as well. This configuration limited direct contact between microorganisms and carbon, as shown in the high-magnification SEM images (Figure S5a,c), where abundant iron oxide minerals surround the microorganisms. In addition, it limited the contact between outer-layer microbes and inner-layer iron oxides. Furthermore, low-magnification photos show that under low carbon conditions (C/Fe = 5:7), PEC exhibits greater ferrihydrite aggregation compared to YP (Figure S6a,c), which correlates with the lower Fe(III) reduction rate and total Fe(II) production observed in Figure 1. This may be due to the more negative zeta potential of PEC compared to YP (Figure 3b).

In contrast, in incubations with a high activated carbon-to-iron ratio (C/Fe = 100:7) in which carbon is abundant and iron is limited, ferrihydrite did not aggregate but was instead dispersed on the surface of the activated carbon (Figure 3a). Microorganisms were also dispersed and adhere to the surface of activated carbon, with sparse ferrihydrite visible on the microbial surfaces, as shown in the high-magnification SEM images in Figure S5b,d. This indicates effective contact between the microorganisms, carbon material, and ferrihydrite. Low-magnification photographs (Figure S6) offer a broader view, demonstrating that the observed phenomenon is widespread. Correspondingly, these high activated carbon-to-iron ratio treatments exhibit quick Fe(III) reduction rates and higher total Fe(II) production (Figure 1c,d). These results preliminarily verified our hypothesis that microstructure of activated carbon−iron oxide aggregates is the key switch that triggers carbonaceous materials to either promote or inhibit microbial iron reduction.

To validate this phenomenon, we conducted a comparative study using *Geobacter sulfurreducens* PCA, which relies on

https://doi.org/10.1021/acs.est.4c14024
Environ. Sci. Technol. 2025, 59, 9576−9586

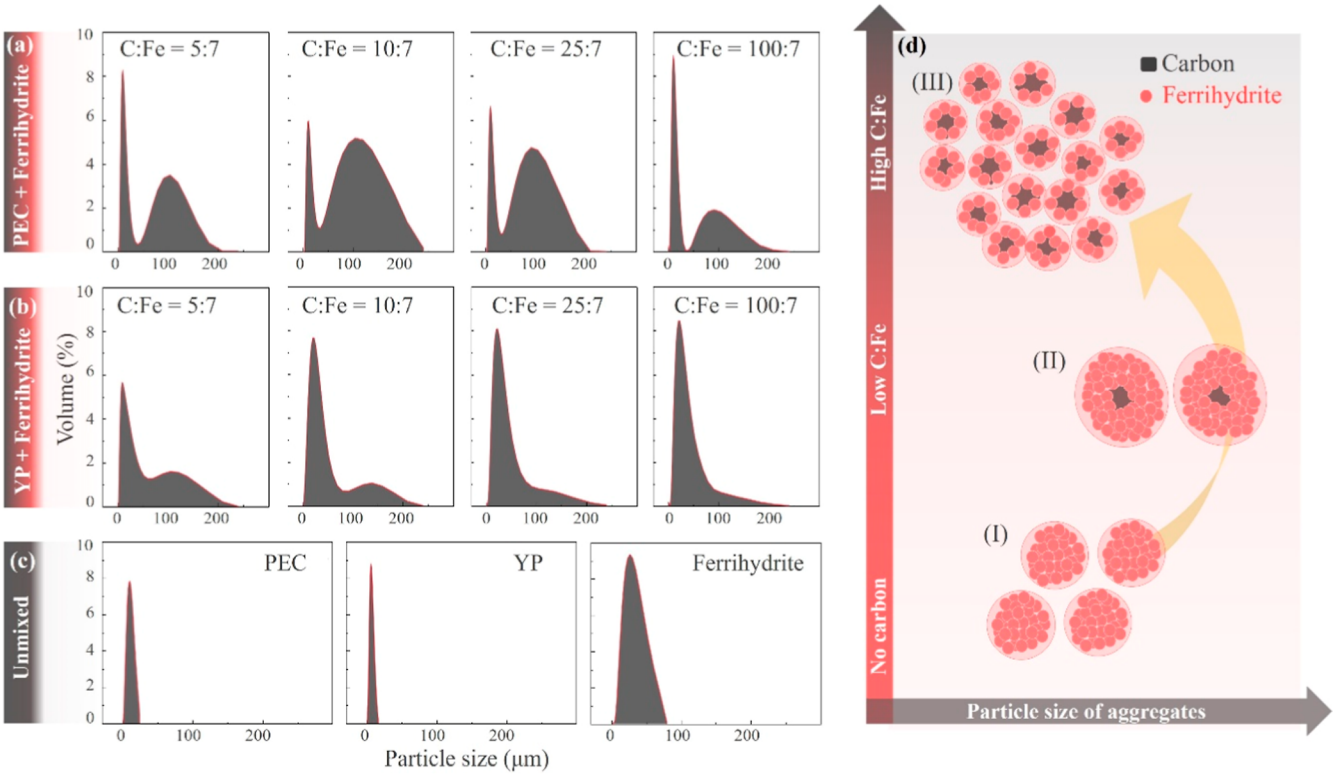

Figure 4. Particle size distribution under different carbon-to-iron ratio conditions. (a) PEC mixed with ferrihydrite; (b) YP mixed with ferrihydrite; (c) particle size distribution of individual PEC, YP, and ferrihydrite samples. A (d) proposed mechanism for the changes in particle size and thickness of the ferrihydrite coating on carbon materials with increasing C/Fe ratio. The particle size was measured after mixing carbon materials with ferrihydrite and allowing 3 days for aggregation equilibrium.

nanowires and direct electron transfer for iron reduction. The trend of iron reduction in the *Geobacter* system, from no enhancement to enhancement, mirrors that in the *Shewanella* system (Figure S7). In addition to the activated carbon materials PEC and YP, we tested 3 types of biochar, and the results were consistent: a low carbon-to-iron ratio did not promote the reaction, while a high ratio did (Figure S8). This supports the existence of a physical interaction mechanism governing promotion and inhibition. However, unlike the *Shewanella* system, the inhibitory effect in *Geobacter* becomes less pronounced with low carbon. SEM images (Figure S9) show that iron−carbon aggregation in the *Geobacter* system (as observed from the wide-field view) is less pronounced than that in the *Shewanella* system (compare with Figure S6a), which may explain the weaker inhibition. Differences in media composition, buffering agents (*Geobacter* uses a carbonate-based medium), or bacterial surface properties may influence aggregation. Significant inhibition occurs only when aggregation is intense, whereas weaker aggregation results in a neutral effect—neither promoting nor inhibiting iron reduction. This may explain the irregular patterns of inhibition and promotion observed in previous studies.

In earlier studies, researchers proposed that activated carbon materials adsorb bacteria cells.[30] This adsorption reduced the cell concentration in suspension and decreased direct contact between the microorganisms and iron oxides. However, based on the zeta potential of activated carbon, microbial cells, and ferrihydrite (Figure 3b), the previous models cannot explain the physical contact between cells, activated carbon and ferrihydrite in our incubations. Zeta potentials for PEC, YP, and the microbial cells are negative, specifically −24 ± 1.8, −18 ± 1.7, and −4.4 ± 0.62 mV, respectively. In contrast, the zeta potential of ferrihydrite is positive, at +9.7 ± 1.2 mV. This indicates that activated carbon is likely to preferentially aggregate with ferrihydrite due to their opposite charges, rather than that with bacteria. Therefore, we propose a cell-activated carbon contact model, as shown in Figure 3c. Activated carbon may primarily impact the contact between microorganisms and iron oxides by influencing the aggregation of ferrihydrite on the surface of the carbon materials. The extent of aggregation, regulated by the iron-to-carbon ratio, will determine whether it promotes or inhibits Fe(III) reduction.

Quantitative Aggregate Size Analysis Explains the Switch Mechanism. We quantified the size of carbon−iron aggregates. Figure 4a,b shows the particle size distributions of PEC and YP mixed with ferrihydrite, while Figure 4c presents those of PEC, YP, and ferrihydrite alone. In the absence of carbon, ferrihydrite particles ranged from 1.9 to 80 μm, with a peak at ∼26 μm. PEC and YP exhibited smaller size ranges of 0.4 to 16.4 μm and 0.5 to 24.1 μm, respectively (Figure 4c). When carbon materials are mixed with ferrihydrite (Figure 4a,b), a strong peak persisted at 0−40 μm, likely corresponding to carbon materials and partially to weakly aggregated ferrihydrite. Notably, a new peak above 100 μm emerged, which likely represents newly formed carbon−iron aggregates, as inferred from the particle size data (Figure 4c) and SEM images (Figure 3a). The intensity of the peak above 100 μm decreased as the carbon-to-iron ratio increased, indicating that higher carbon content reduces aggregate size. This observation aligns with SEM results, which show that under high carbon-to-iron ratio conditions, ferrihydrite transitions to sparsely

https://doi.org/10.1021/acs.est.4c14024
Environ. Sci. Technol. 2025, 59, 9576−9586

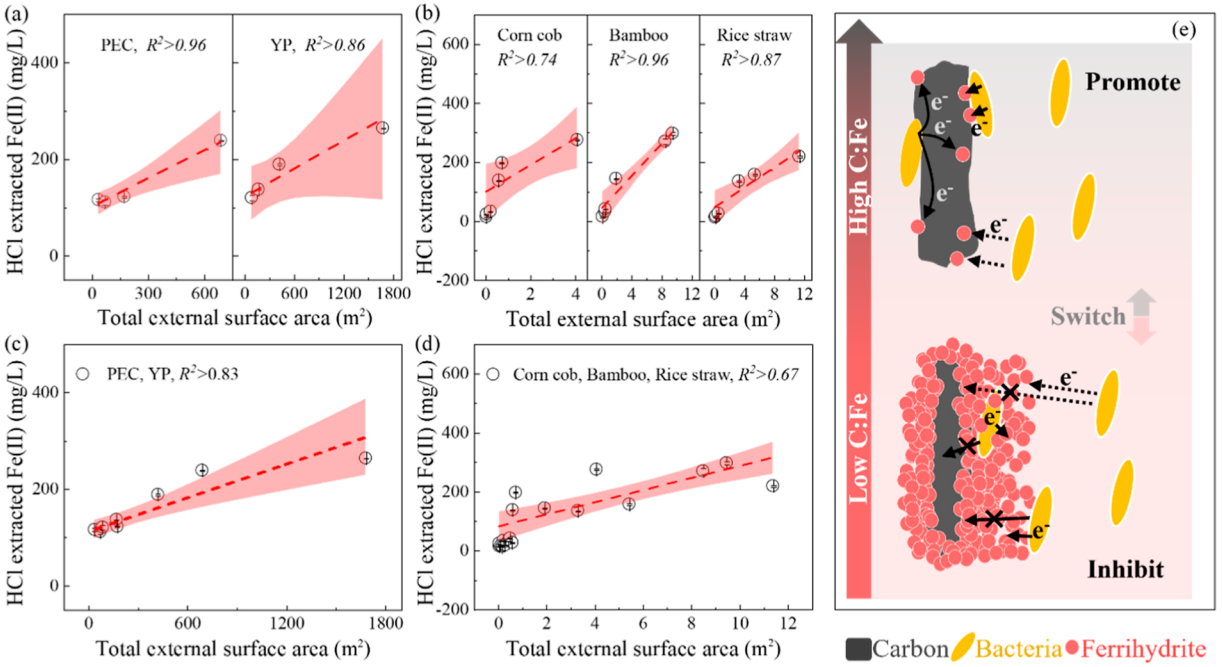

Figure 5. Correlation between microbial Fe(III) reduction and total external surface area. (a) PEC and YP individually; (b) biochar from corn cob, bamboo, and rice straw individually, without distinguishing pyrolysis temperatures; (c) correlation of PEC and YP combined, without distinguishing material sources; (d) correlation of 9 biochars combined, without distinguishing sources or pyrolysis temperatures; (e) schematic diagram of the promotion and inhibition switch mechanism proposed in this study. The external surface area was calculated as the difference between total surface area and pore area, using BET analysis. The total external surface area is calculated by multiplying the external surface area per unit mass by the amount added.

attached cluster on carbon surfaces. Together, these findings demonstrate that under low-carbon conditions, ferrihydrite forms large aggregates, whereas under high-carbon conditions, it disperses across carbon materials.

The specific surface area of samples with different carbon-to-iron ratios was further tested using the BET technique. The results show that as the carbon-to-iron ratio increases, the specific surface area gradually increases from 523 m^2/g (PEC) and 718 m^2/g (YP) to 1341 m^2/g (PEC) and 1725 m^2/g (YP) (Table S2), approaching the intrinsic specific surface area of PEC and YP (1885 and 2276 m^2/g, respectively) (Table S3). This increase in specific surface area is consistent with the observed decrease in the particle size. Moreover, these surface area correlates positively with iron reduction rates (Figure S10), highlighting the critical role of aggregate size in microbial Fe(III) reduction.

Based on the above results, we propose a physical interaction mechanism for the changes in particle size when carbon and iron coexist, as shown in Figure 4d. When ferrihydrite exists alone, it can aggregate to some extent, as shown in state (I). However, due to the more negative zeta potential of the carbon materials, when a small amount of carbon materials come into contact with ferrihydrite, a larger aggregate structure of iron coated with carbon forms, and the aggregate particle size increases, as shown in state (II). Collectively, the larger particles have a lower total surface area and microorganisms cannot interact with the iron-encased carbon particles. As the carbon-to-iron ratio continues to rise, the total surface area of the carbon gradually increases, causing ferrihydrite to disperse on the surface of the carbon materials, which leads to smaller aggregate particles, as shown in state (III). This process is similar to the previously reported effects of humic substances on the aggregation of ferrihydrite,[24] further suggesting that it may be a common behavior when ferrihydrite interacts with various elements in the natural environment. This change in the physical interaction mechanism explains the observed shift in the effect of carbon materials on iron reduction from inhibition to promotion.

Total External Surface Area Determines Electron Transfer Rate and Extent. The total external surface area of the carbon materials (specific surface area × total amount added) is likely a key factor influencing both the rate and extent of Fe(III) reduction. This is because the pores of the carbon materials are primarily on the nanometer scale, while ferrihydrite aggregates range from 1.4 to 80 μm, suggesting that ferrihydrite likely attaches to the external surface of the carbon materials. Based on the SEM (Figure 3) and particle size quantification results (Figure 4) mentioned above, which suggest that iron aggregation on carbon to form "iron-coated carbon" may be a key factor affecting the iron reduction rate, we hypothesized that the external surface area of carbon materials is a critical parameter influencing aggregation and Fe(III) reduction. Therefore, we performed a correlation analysis between the total external surface area of carbon materials and Fe(III) reduction rates in different reaction systems.

Furthermore, to verify the general applicability of this relationship across a broader range of carbonaceous materials, we included an expanded set of carbon samples for correlation analysis, comprising 9 types of biochar derived from different sources (corn cob, rice straw, and bamboo) and pyrolyzed at various temperatures (600, 800, and 1000 °C). SEM images of the interactions between all 9 types of biochar and iron oxides (Figures S11−S13) exhibited patterns similar to those of activated carbon shown in Figure 3. Specifically, carbon was encapsulated by ferrihydrite at low biochar carbon-to-iron

https://doi.org/10.1021/acs.est.4c14024
Environ. Sci. Technol. 2025, 59, 9576−9586

ratios, while ferrihydrite was dispersed on the biochar surfaces at high biochar carbon-to-iron ratios. BET-determined, specific surface areas of all carbonaceous materials used in this study are presented in Table S3. The total surface areas and total external surface areas of the two activated carbons and 9 biochars, calculated by multiplying the area per unit mass by the amount added in each experiment, are shown in Tables S4−S7. Their zeta potentials, as shown in Table S8, are all negative. For the biochar materials, we measured the amount of Fe(III) reduction before the reaction reached steady-state (at 6 h, OD_{600} = 0.5) for correlation analysis, as shown in Figure S14. We used this value to represent the Fe(III) reduction rate of each incubation. The results of the correlation analysis are shown in Figure 5a−d.

We categorized the materials from 5 different sources and conducted separate correlation analyses for each group. The results revealed a strong positive correlation between the amount of Fe(III) reduction and the total external surface area across all cases (Figure 5a,b). The correlation coefficients were as follows: PEC R^2 = 0.96, YP R^2 = 0.86, biochar-corn cob R^2 = 0.74, biochar-bamboo R^2 = 0.96, and biochar-rice straw R^2 = 0.87. The correlation coefficients for biochar were slightly lower than those for activated carbon, likely because each group of biochar includes materials produced at three different pyrolysis temperatures. Nevertheless, the correlations were still significant. Then, we performed correlation analyses across all activated carbon materials and all biochar materials, without distinguishing between their sources. The positive correlation between iron reduction and total external surface area remained significant (activated carbon R^2 = 0.83; biochar R^2 = 0.67) (Figure 5c,d). Although the infrared characterization shows significant differences in the surface functional groups of the different biochars we selected (Figure S15), the promotion and inhibition mechanisms they exhibit remain consistent. These materials, derived from different raw materials and processed at various temperatures, exhibited differences in surface functional groups, conductivity (Table S9), and dissolved leachates, yet the correlation remained strong, highlighting the importance of external surface area as a key factor influencing Fe(III) reduction.

These results strongly demonstrate the universality of this mechanism: although there are differences in chemical structure and conductivity among various carbonaceous materials, whether they mediate electron transfer through electron shuttling or conductivity, the physical contact of cells with carbon material remains the most critical factor determining whether they promote or inhibit Fe(III) reduction. It reveals a key mechanism that determines whether carbonaceous materials promote or inhibit microbial Fe(III) reduction, as shown in the model presented in Figure 5e. After carbon materials aggregate with iron oxides, internal ferrihydrite becomes inactive, leading to a decline in both the rate and extent of Fe(III) reduction. As the activated or biochar carbon-to-iron oxide ratio increases, although the carbon material still adsorbs ferrihydrite and causes aggregation, ferrihydrite can no longer occupy all the sites on the surface of the carbon material but instead sparsely adheres to the surface. At this point, whether microorganisms are suspended in the solution or attached to the surfaces of iron or carbon, they can effectively transfer electrons to the ferrihydrite on the carbon surface through direct contact, electron shuttling, or conductive transfer, leading to a significant increase in Fe(III) reduction rates. While the conductivity of carbon materials can accelerate electron transfer between microorganisms and iron oxides, biochar with low conductivity (at 600 °C) and rich in surface functional groups also shows good iron reduction performance. Therefore, it is still unclear whether direct conductivity or surface functional groups contribute more to electron transfer in this system. However, our results confirm that the effective dispersion of iron oxide on the carbon surface is essential for the enhancement of these reactions, highlighting the importance of considering the spatial configurations of solid phase reactants in heterogeneous aggregate−microbe systems. For over a decade, the promoting and inhibiting effects of materials like biochar and activated carbon on microbial Fe(III) reduction have been a subject of debate. The mechanism elucidated in this study may help resolve this important scientific question.

■ ENVIRONMENTAL IMPLICATIONS

In 2014, pyrolytic carbon (biochar) was first reported to act as a solid-state electron shuttle, accelerating electron transfer between microorganisms and iron oxides.[12] Over the following decade, a series of studies emerged on biochar, black carbon, and activated carbon-mediated electron transfer. These include research on biochar promoting interspecies electron transfer,[66] biochar-mediated anaerobic methane oxidation,[67] biochar accelerating N_2O emissions,[68,69] and high-temperature pyrolyzed carbon enhancing microbial electron transfer through its inherent conductivity.[63] Although the concept of "biochar promoting microbial Fe(III) mineral reduction" became widely recognized, some subsequent studies reported cases where biochar inhibited microbial Fe(III) reduction. For instance, low concentrations of biochar inhibited ferrihydrite reduction,[30] and biochar with adsorbed microorganisms inhibited nontronite reduction.[31] To date, no research has systematically addressed the factors controlling the "switch" by which pyrolyzed carbon and activated carbon either promote or inhibit microbial Fe(III) reduction. Early studies reported that phosphate and humic substances inhibited microbial iron reduction, with the authors attributing this to increased aggregation of ferrihydrite.[24] Recent studies have shown that activated carbon inhibits iron reduction and methane emissions in soil, contradicting the previous understanding that carbon materials promote iron reduction by virtue of their conductivity. Lower iron reduction was mainly due to activated carbon strongly adsorbing soil DOM, reducing available carbon sources and electron shuttles.[4] The inhibition of respiration by DOM adsorbed on activated carbon particles is consistent with the viewpoint that "physical interaction is critical", as proposed in this study. Our study proposes the theory of "physical contact: the key switch triggering carbonaceous materials to promote microbial Fe(III) mineral reduction" and validates the universality of this process using 11 different types of carbonaceous materials, including activated carbons and biochars. This mechanism partially addresses the debate over whether carbonaceous materials promote or inhibit Fe(III) mineral reduction. This work has significant implications for advancing the understanding of the fundamental properties of both activated carbon and pyrolytic carbon, as well as the theory of microbial Fe(III) reduction.

■ ASSOCIATED CONTENT

Data Availability Statement

Supporting data to this article can be found online.

https://doi.org/10.1021/acs.est.4c14024
Environ. Sci. Technol. 2025, 59, 9576−9586

Supporting Information

The Supporting Information is available free of charge at https://pubs.acs.org/doi/10.1021/acs.est.4c14024.

Materials preparation; description about the impact of activated carbon on ferrihydrite transformation; chemical analysis methods; BET specific surface area; total surface area; total external surface area; zeta potential; electrical conductivity; Fe(III) reduction kinetics under different cell densities; mineral transformation changes caused by adsorption; Fe(III) reduction after pyrolysis of the material at 1000 °C; rate constant after washing; high-magnification SEM; low-magnification SEM; Fe(III) mineral reduction kinetics of *Geobacter*; Fe(III) reduction capacity of biochars at low carbon−iron ratio and high iron ratio; SEM of *Geobacter*; correlation between aggregate surface area and reduction rate; SEM of biochar; Fe(III) reduction in the biochar system; and Fourier transform infrared spectroscopy (PDF)

AUTHOR INFORMATION

Corresponding Author

Yundang Wu − *National-Regional Joint Engineering Research Center for Soil Pollution Control and Remediation in South China, Guangdong Key Laboratory of Integrated Agro-environmental Pollution Control and Management, Institute of Eco-environmental and Soil Sciences, Guangdong Academy of Sciences, Guangzhou 510650, China;* orcid.org/0000-0003-2996-5407; Phone: 020-87025180; Email: ydwu@soil.gd.cn

Authors

Lin Shen − *Guangzhou Institute of Geochemistry, Chinese Academy of Sciences, Guangzhou 510640, China; National-Regional Joint Engineering Research Center for Soil Pollution Control and Remediation in South China, Guangdong Key Laboratory of Integrated Agro-environmental Pollution Control and Management, Institute of Eco-environmental and Soil Sciences, Guangdong Academy of Sciences, Guangzhou 510650, China; University of Chinese Academy of Sciences, Beijing 100049, China*

Xiao Zhu − *Guangzhou Institute of Geochemistry, Chinese Academy of Sciences, Guangzhou 510640, China; National-Regional Joint Engineering Research Center for Soil Pollution Control and Remediation in South China, Guangdong Key Laboratory of Integrated Agro-environmental Pollution Control and Management, Institute of Eco-environmental and Soil Sciences, Guangdong Academy of Sciences, Guangzhou 510650, China; University of Chinese Academy of Sciences, Beijing 100049, China*

Haoze Jiang − *School of Environment and Chemical Engineering, Foshan University, Foshan 528000, China*

Juntao Zhang − *Guangzhou Institute of Forestry and Landscape Architecture, Guangzhou 510405, China*

Chengyu Chen − *College of Natural Resources and Environment, Guangdong Provincial Key Laboratory of Agricultural & Rural Pollution Abatement and Environmental Safety, South China Agricultural University, Guangzhou 510642, China;* orcid.org/0000-0003-2597-471X

John R. Reinfelder − *Department of Environmental Sciences, Rutgers University, New Brunswick, New Jersey 08901, United States*

Andreas Kappler − *Geomicrobiology, Department of Geoscience, University of Tübingen, Tübingen 72076, Germany; Cluster of Excellence EXC 2124, Controlling Microbes to Fight Infection, Tübingen University, Tübingen 72076, Germany;* orcid.org/0000-0002-3558-9500

Liping Fang − *National-Regional Joint Engineering Research Center for Soil Pollution Control and Remediation in South China, Guangdong Key Laboratory of Integrated Agro-environmental Pollution Control and Management, Institute of Eco-environmental and Soil Sciences, Guangdong Academy of Sciences, Guangzhou 510650, China*

Tongxu Liu − *National-Regional Joint Engineering Research Center for Soil Pollution Control and Remediation in South China, Guangdong Key Laboratory of Integrated Agro-environmental Pollution Control and Management, Institute of Eco-environmental and Soil Sciences, Guangdong Academy of Sciences, Guangzhou 510650, China;* orcid.org/0000-0002-2348-3952

Chuanping Liu − *National-Regional Joint Engineering Research Center for Soil Pollution Control and Remediation in South China, Guangdong Key Laboratory of Integrated Agro-environmental Pollution Control and Management, Institute of Eco-environmental and Soil Sciences, Guangdong Academy of Sciences, Guangzhou 510650, China*

Fangbai Li − *National-Regional Joint Engineering Research Center for Soil Pollution Control and Remediation in South China, Guangdong Key Laboratory of Integrated Agro-environmental Pollution Control and Management, Institute of Eco-environmental and Soil Sciences, Guangdong Academy of Sciences, Guangzhou 510650, China;* orcid.org/0000-0001-9027-9313

Complete contact information is available at: https://pubs.acs.org/10.1021/acs.est.4c14024

Notes

The authors declare no competing financial interest.

ACKNOWLEDGMENTS

This work was funded by the National Natural Science Foundations of China (42321005, 42077020, 42377315, 42377398), the National Key Research and Development Program (2023YFD1902100, 2023YFD1901300), the GDAS' Project of Science and Technology Development (2023GDASQNRC-0202), Key-Area Research and Development Program of Guangdong Province (2023B0202010027), and Guangdong Basic and Applied Basic Research Foundation (2023B030300006).

REFERENCES

(1) Zou, X.; Cao, K.; Wang, Q.; Kang, S.; Wang, Y. Enhanced Degradation of Polylactic Acid Microplastics in Acidic Soils: Does the Application of Biochar Matter? *J. Hazard. Mater.* **2024**, *477*, 135262.

(2) Shi, R.; Hong, Z.; Li, J.; Jiang, J.; Baquy, M. A.-A.; Xu, R.; Qian, W. Mechanisms for Increasing the pH Buffering Capacity of an Acidic Ultisol by Crop Residue-Derived Biochars. *J. Agric. Food Chem.* **2017**, *65* (37), 8111−8119.

(3) Yang, L.; Yang, X.; Guo, J.; Yang, Z.; Du, Y.; Lu, Q.; Zhong, G. Invasive Plant-Derived Biochar for Sustainable Bioremediation of Pesticide Contaminated Soil. *Chem. Eng. J.* **2024**, *481*, 148689.

(4) Si, D.; Wu, S.; Wu, H.; Wang, D.; Fu, Q.; Wang, Y.; Wang, P.; Zhao, F.; Zhou, D. Activated Carbon Application Simultaneously Alleviates Paddy Soil Arsenic Mobilization and Carbon Emission by Decreasing Porewater Dissolved Organic Matter. *Environ. Sci. Technol.* **2024**, *58* (18), 7880−7890.

(5) Chi, W.; Nan, Q.; Liu, Y.; Dong, D.; Qin, Y.; Li, S.; Wu, W. Stress Resistance Enhancing with Biochar Application and Promotion on Crop Growth. *Biochar* **2024**, *6* (1), 43.
(6) Liu, Z.; Xu, Z.; Xu, L.; Buyong, F.; Chay, T. C.; Li, Z.; Cai, Y.; Hu, B.; Zhu, Y.; Wang, X. Modified Biochar: Synthesis and Mechanism for Removal of Environmental Heavy Metals. *Carbon Res.* **2022**, *1* (1), 8.
(7) Sharma, K.; Sharma, P.; Sangwan, P. Bioremediation of RDX and HMX Contaminated Soil Employing a Biochar-Based Bioformulation. *Carbon Res.* **2023**, *2*, 33.
(8) Zhou, S.; Qi, X.; Tang, Y.; Yu, W.; Guan, Q.; Bu, Y.; Tan, L.; Gu, G. Activated Carbon-Mediated Arsenopyrite Oxidation and Arsenic Immobilization: ROS Formation and Its Role. *J. Hazard. Mater.* **2024**, *480*, 135917.
(9) Huang, F.; Dong, F.; Chen, L.; Zeng, Y.; Zhou, L.; Sun, S.; Wang, Z.; Lai, J.; Fang, L. Biochar-Mediated Remediation of Uranium-Contaminated Soils: Evidence, Mechanisms, and Perspectives. *Biochar* **2024**, *6*, 16.
(10) Li, Y.; Abdo, A. I.; Shi, Z.; Merwad, A.-R. M. A.; Zhang, J. Biochar Derived from Invasive Plants Improved the pH, Macronutrient Availability and Biological Properties Better than Liming for Acid Rain-Affected Soil. *Biochar* **2023**, *5* (1), 59.
(11) Bolan, N.; Sarmah, A. K.; Bordoloi, S.; Bolan, S.; Padhye, L. P.; Van Zwieten, L.; Sooriyakumar, P.; Khan, B. A.; Ahmad, M.; Solaiman, Z. M.; Rinklebe, J.; Wang, H.; Singh, B. P.; Siddique, K. H. M. Soil Acidification and the Liming Potential of Biochar. *Environ. Pollut.* **2023**, *317*, 120632.
(12) Kappler, A.; Wuestner, M. L.; Ruecker, A.; Harter, J.; Halama, M.; Behrens, S. Biochar as an Electron Shuttle between Bacteria and Fe(III) Minerals. *Environ. Sci. Technol. Lett.* **2014**, *1* (8), 339−344.
(13) He, H.; Liu, J.; Shu, Z.; Chen, Y.; Pan, Z.; Peng, C.; Wang, X.; Zhou, F.; Zhou, M.; Du, Z.; Sun, K.; Xing, B.; Wang, Z. Microbially Driven Iron Cycling Facilitates Organic Carbon Accrual in Decadal Biochar-Amended Soil. *Environ. Sci. Technol.* **2024**, *58* (28), 12430−12440.
(14) Wu, S.; Fang, G.; Wang, Y.; Zheng, Y.; Wang, C.; Zhao, F.; Jaisi, D. P.; Zhou, D. Redox-Active Oxygen-Containing Functional Groups in Activated Carbon Facilitate Microbial Reduction of Ferrihydrite. *Environ. Sci. Technol.* **2017**, *51* (17), 9709−9717.
(15) Ren, J.; Huang, H.; Zhang, Z.; Xu, X.; Zhao, L.; Qiu, H.; Cao, X. Enhanced Microbial Reduction of Cr(VI) in Soil with Biochar Acting as an Electron Shuttle: Crucial Role of Redox-Active Moieties. *Chemosphere* **2023**, *328*, 138601.
(16) Ren, S.; Usman, M.; Tsang, D. C. W.; O-Thong, S.; Angelidaki, I.; Zhu, X.; Zhang, S.; Luo, G. Hydrochar-Facilitated Anaerobic Digestion: Evidence for Direct Interspecies Electron Transfer Mediated through Surface Oxygen-Containing Functional Groups. *Environ. Sci. Technol.* **2020**, *54* (9), 5755−5766.
(17) Zhang, P.; Liu, A.; Huang, P.; Min, L.; Sun, H. Sorption and Molecular Fractionation of Biochar-Derived Dissolved Organic Matter on Ferrihydrite. *J. Hazard. Mater.* **2020**, *392*, 122260.
(18) Zhang, P.; Meng, X.; Liu, A.; Ma, M.; Shao, Y.; Sun, H. Biochar-Derived Dissolved Black Carbon Accelerates Ferrihydrite Microbial Transformation and Subsequent Imidacloprid Degradation. *J. Hazard. Mater.* **2023**, *446*, 130685.
(19) Xu, S.; Adhikari, D.; Huang, R.; Zhang, H.; Tang, Y.; Roden, E.; Yang, Y. Biochar-Facilitated Microbial Reduction of Hematite. *Environ. Sci. Technol.* **2016**, *50* (5), 2389−2395.
(20) Li, L.; Gao, Q.; Liu, X.; Zhao, Q.; Wang, W.; Wang, K.; Zhou, H.; Jiang, J. Insights into High-Solids Anaerobic Digestion of Food Waste Enhanced by Activated Carbon via Promoting Direct Interspecies Electron Transfer. *Bioresour. Technol.* **2022**, *351*, 127008.
(21) Rotaru, A.-E.; Shrestha, P. M.; Liu, F.; Markovaite, B.; Chen, S.; Nevin, K. P.; Lovley, D. R. Direct Interspecies Electron Transfer between Geobacter Metallireducens and Methanosarcina Barkeri. *Appl. Environ. Microbiol.* **2014**, *80* (15), 4599−4605.
(22) Qiao, J.-t.; Li, X.; Hu, M.; Li, F.; Young, L. Y.; Sun, W.; Huang, W.; Cui, J. Transcriptional Activity of Arsenic-Reducing Bacteria and Genes Regulated by Lactate and Biochar during Arsenic Transformation in Flooded Paddy Soil. *Environ. Sci. Technol.* **2018**, *52*, 61−70.
(23) Bar-Or, I.; Elvert, M.; Eckert, W.; Kushmaro, A.; Vigderovich, H.; Zhu, Q.; Ben-Dov, E.; Sivan, O. Iron-Coupled Anaerobic Oxidation of Methane Performed by a Mixed Bacterial-Archaeal Community Based on Poorly Reactive Minerals. *Environ. Sci. Technol.* **2017**, *51* (21), 12293−12301.
(24) Amstaetter, K.; Borch, T.; Kappler, A. Influence of Humic Acid Imposed Changes of Ferrihydrite Aggregation on Microbial Fe(III) Reduction. *Geochim. Cosmochim. Acta* **2012**, *85*, 326−341.
(25) Liu, Y.; Ma, J.; Gao, J.; Chen, X.; Ouyang, X.; Weng, L.; Li, H.; Chen, Y.; Li, Y. Stability and Interaction of Biochar and Iron Mineral Nanoparticles: Effect of pH, Ionic Strength, and Dissolved Organic Matter. *Biochar* **2022**, *4* (1), 47.
(26) Wang, D.; Zhang, W.; Zhou, D. Antagonistic Effects of Humic Acid and Iron Oxyhydroxide Grain-Coating on Biochar Nanoparticle Transport in Saturated Sand. *Environ. Sci. Technol.* **2013**, *47* (10), 5154−5161.
(27) Yan, C.; Li, Y.; Sharma, P.; Chen, Q.; Li, B.; Shang, J. Influence of Dissolved Organic Matter, Kaolinite, and Iron Oxides on Aggregation and Transport of Biochar Colloids in Aqueous and Soil Environments. *Chemosphere* **2022**, *306*, 135555.
(28) Weng, Y.-T.; Rathod, J.; Liang, B.; Wang, C.-C.; Iizuka, Y.; Tamura, N.; Chen, C.-L.; Lee, Y.-C. Black Carbon Enriches Short-Range-Order Ferrihydrite in Amazonian Dark Earth: Interplay Mechanism and Environmental Implications. *Sci. Total Environ.* **2020**, *725*, 138195.
(29) Wang, D.; Root, R. A.; Chorover, J. Biochar-Templated Surface Precipitation and Inner-Sphere Complexation Effectively Removes Arsenic from Acid Mine Drainage. *Environ. Sci. Pollut. Res.* **2021**, *28* (33), 45519−45533.
(30) Yang, Z.; Sun, T.; Subdiaga, E.; Obst, M.; Haderlein, S. B.; Maisch, M.; Kretzschmar, R.; Angenent, L. T.; Kappler, A. Aggregation-Dependent Electron Transfer via Redox-Active Biochar Particles Stimulate Microbial Ferrihydrite Reduction. *Sci. Total Environ.* **2020**, *703*, 135515.
(31) Dong, H.; Coffin, E. S.; Sheng, Y.; Duley, M. L.; Khalifa, Y. M. Microbial Reduction of Fe(III) in Nontronite: Role of Biochar as a Redox Mediator. *Geochim. Cosmochim. Acta* **2023**, *345*, 102−116.
(32) Tan, Z.; Yuan, S.; Hong, M.; Zhang, L.; Huang, Q. Mechanism of Negative Surface Charge Formation on Biochar and Its Effect on the Fixation of Soil Cd. *J. Hazard. Mater.* **2020**, *384*, 121370.
(33) Song, B.; Chen, M.; Zhao, L.; Qiu, H.; Cao, X. Physicochemical Property and Colloidal Stability of Micron- and Nano-Particle Biochar Derived from a Variety of Feedstock Sources. *Sci. Total Environ.* **2019**, *661*, 685−695.
(34) Cai, W.; Bordoloi, S.; Ng, C. W. W.; Sarmah, A. K. Influence of Pore Fluid Salinity on Shrinkage and Water Retention Characteristics of Biochar Amended Kaolin for Landfill Liner Application. *Sci. Total Environ.* **2022**, *838*, 156493.
(35) Farhangi-Abriz, S.; Ghassemi-Golezani, K. Improving Electrochemical Characteristics of Plant Roots by Biochar Is an Efficient Mechanism in Increasing Cations Uptake by Plants. *Chemosphere* **2023**, *313*, 137365.
(36) De Bhowmick, G.; Briones, R. M.; Thiele-Bruhn, S.; Sen, R.; Sarmah, A. K. Adsorptive Removal of Metformin on Specially Designed Algae-Lignocellulosic Biochar Mix and Techno-Economic Feasibility Assessment. *Environ. Pollut.* **2022**, *292*, 118256.
(37) Li, X.; Yang, P.; Zhao, W.; Guo, F.; Jaisi, D. P.; Mi, S.; Ma, H.; Lin, B.; Feng, X.; Tan, W.; Wang, X. Adsorption Mechanisms of Glyphosate on Ferrihydrite: Effects of Al Substitution and Aggregation State. *Environ. Sci. Technol.* **2023**, *57* (38), 14384−14395.
(38) Liu, X.; Wang, Y.; Xiang, H.; Wu, J.; Yan, X.; Zhang, W.; Lin, Z.; Chai, L. Unveiling the Crucial Role of Iron Mineral Phase Transformation in Antimony(V) Elimination from Natural Water. *Eco-Environ. Health* **2023**, *2* (3), 176−183.
(39) Yi, P.; Pignatello, J. J.; Uchimiya, M.; White, J. C. Heteroaggregation of Cerium Oxide Nanoparticles and Nanoparticles

of Pyrolyzed Biomass. *Environ. Sci. Technol.* **2015**, *49* (22), 13294−13303.
(40) Liu, Y.; Ding, Y.; Sheng, A.; Li, X.; Chen, J.; Arai, Y.; Liu, J. Fe(II)-Catalyzed Transformation of Ferrihydrite with Different Degrees of Crystallinity. *Environ. Sci. Technol.* **2023**, *57* (17), 6934−6943.
(41) Qafoku, O.; Kovarik, L.; Bowden, M. E.; Nakouzi, E.; Sheng, A.; Liu, J.; Pearce, C. I.; Rosso, K. M. Nanoscale Observations of Fe(II)-Induced Ferrihydrite Transformation. *Environ. Sci.: Nano* **2020**, *7* (10), 2953−2967.
(42) Liu, F.; Rotaru, A.-E.; Shrestha, P. M.; Malvankar, N. S.; Nevin, K. P.; Lovley, D. R. Promoting Direct Interspecies Electron Transfer with Activated Carbon. *Energy Environ. Sci.* **2012**, *5* (10), 8982−8989.
(43) Tessmer, C. H.; Vidic, R. D.; Uranowski, L. J. Impact of Oxygen-Containing Surface Functional Groups on Activated Carbon Adsorption of Phenols. *Environ. Sci. Technol.* **1997**, *31* (7), 1872−1878.
(44) Kearns, J. P.; Wellborn, L. S.; Summers, R. S.; Knappe, D. R. U. 2,4-D Adsorption to Biochars: Effect of Preparation Conditions on Equilibrium Adsorption Capacity and Comparison with Commercial Activated Carbon Literature Data. *Water Res.* **2014**, *62*, 20−28.
(45) Wu, Y.; Zhu, X.; Wang, X.; Lin, Z.; Reinfelder, J. R.; Li, F.; Liu, T. A New Electron Shuttling Pathway Mediated by Lipophilic Phenoxazine via the Interaction with Periplasmic and Inner Membrane Proteins of *Shewanella Oneidensis* MR-1. *Environ. Sci. Technol.* **2023**, *57* (6), 2636−2646.
(46) Michel, F. M.; Ehm, L.; Antao, S. M.; Lee, P. L.; Chupas, P. J.; Liu, G.; Strongin, D. R.; Schoonen, M. A. A.; Phillips, B. L.; Parise, J. B. The Structure of Ferrihydrite, a Nanocrystalline Material. *Science* **2007**, *316*, 1726−1729.
(47) Wu, C.; An, W.; Liu, Z.; Lin, J.; Qian, Z.; Xue, S. The Effects of Biochar as the Electron Shuttle on the Ferrihydrite Reduction and Related Arsenic (As) Fate. *J. Hazard. Mater.* **2020**, *390*, 121391.
(48) Yang, Z.; Sun, T.; Kappler, A.; Jiang, J. Biochar Facilitates Ferrihydrite Reduction by Shewanella Oneidensis MR-1 through Stimulating the Secretion of Extracellular Polymeric Substances. *Sci. Total Environ.* **2022**, *848*, 157560.
(49) Amstaetter, K.; Borch, T.; Larese-Casanova, P.; Kappler, A. Redox Transformation of Arsenic by Fe(II)-Activated Goethite (r-FeOOH). *Environ. Sci. Technol.* **2010**, *44* (1), 102−108.
(50) Sheng, A.; Liu, J.; Li, X.; Qafoku, O.; Collins, R. N.; Jones, A. M.; Pearce, C. I.; Wang, C.; Ni, J.; Lu, A.; Rosso, K. M. Labile Fe(III) from Sorbed Fe(II) Oxidation Is the Key Intermediate in Fe(II)-Catalyzed Ferrihydrite Transformation. *Geochim. Cosmochim. Acta* **2020**, *272*, 105−120.
(51) Sheng, A.; Li, X.; Arai, Y.; Ding, Y.; Rosso, K. M.; Liu, J. Citrate Controls Fe(II)-Catalyzed Transformation of Ferrihydrite by Complexation of the Labile Fe(III) Intermediate. *Environ. Sci. Technol.* **2020**, *54* (12), 7309−7319.
(52) Sheng, A.; Liu, J.; Li, X.; Luo, L.; Ding, Y.; Chen, C.; Zhang, X.; Wang, C.; Rosso, K. M. Labile Fe(III) Supersaturation Controls Nucleation and Properties of Product Phases from Fe(II)-Catalyzed Ferrihydrite Transformation. *Geochim. Cosmochim. Acta* **2021**, *309*, 272−285.
(53) Liu, J.; Sheng, A.; Li, X.; Arai, Y.; Ding, Y.; Nie, M.; Yan, M.; Rosso, K. M. Understanding the Importance of Labile Fe(III) during Fe(II)-Catalyzed Transformation of Metastable Iron Oxyhydroxides. *Environ. Sci. Technol.* **2022**, *56* (6), 3801−3811.
(54) Piepenbrock, A.; Dippon, U.; Porsch, K.; Appel, E.; Kappler, A. Dependence of Microbial Magnetite Formation on Humic Substance and Ferrihydrite Concentrations. *Geochim. Cosmochim. Acta* **2011**, *75* (22), 6844−6858.
(55) Xu, X.; Huang, H.; Zhang, Y.; Xu, Z.; Cao, X. Biochar as Both Electron Donor and Electron Shuttle for the Reduction Transformation of Cr(VI) during Its Sorption. *Environ. Pollut.* **2019**, *244*, 423−430.
(56) Wu, S.; Fang, G.; Wang, D.; Jaisi, D. P.; Cui, P.; Wang, R.; Wang, Y.; Wang, L.; Sherman, D. M.; Zhou, D. Fate of As(III) and As(V) during Microbial Reduction of Arsenic-Bearing Ferrihydrite Facilitated by Activated Carbon. *ACS Earth Space Chem.* **2018**, *2* (9), 878−887.
(57) Chang, J.; Ren, N.; Yuan, Q.; Wang, S.; Liang, D.; He, Z.; Wang, X.; Li, N. Charging-Discharging Cycles of Geobattery Activated Carbon Enhance Iron Reduction and Vivianite Recovery from Wastewater. *Sci. Total Environ.* **2023**, *882*, 163541.
(58) Bai, Y.; Sun, T.; Angenent, L. T.; Haderlein, S. B.; Kappler, A. Electron Hopping Enables Rapid Electron Transfer between Quinone-/Hydroquinone-Containing Organic Molecules in Microbial Iron(III) Mineral Reduction. *Environ. Sci. Technol.* **2020**, *54*, 10646−10653.
(59) Bai, Y.; Sun, T.; Mansor, M.; Joshi, P.; Zhuang, Y.; Haderlein, S. B.; Fischer, S.; Konhauser, K. O.; Alessi, D. S.; Kappler, A. Networks of Dissolved Organic Matter and Organo-Mineral Associations Stimulate Electron Transfer over Centimeter Distances. *Environ. Sci. Technol. Lett.* **2023**, *10*, 493−498.
(60) Zhang, Y.; Tong, M.; Lu, Y.; Zhao, F.; Zhang, P.; Wan, Z.; Li, P.; Yuan, S.; Wang, Y.; Kappler, A. Directional Long-Distance Electron Transfer from Reduced to Oxidized Zones in the Subsurface. *Nat. Commun.* **2024**, *15*, 6576.
(61) Sun, W.-X.; Fu, S.-F.; Zhu, R.; Wang, Z.-Y.; Zou, H.; Zheng, Y. Improved Anaerobic Digestion Efficiency of High-Solid Sewage Sludge by Enhanced Direct Interspecies Electron Transfer with Activated Carbon Mediator. *Bioresour. Technol.* **2020**, *313*, 123648.
(62) Wang, T.; Zhang, Z.; Gu, Z.; Hu, C.; Qu, J. Electron Transfer of Activated Carbon to Anode Excites and Regulates Desalination in Flow Electrode Capacitive Deionization. *Environ. Sci. Technol.* **2023**, *57* (6), 2566−2574.
(63) Yu, W.; Chu, C.; Chen, B. Enhanced Microbial Ferrihydrite Reduction by Pyrogenic Carbon: Impact of Graphitic Structures. *Environ. Sci. Technol.* **2022**, *56* (1), 239−250.
(64) Jiang, J.; Kappler, A. Kinetics of Microbial and Chemical Reduction of Humic Substances: Implications for Electron Shuttling. *Environ. Sci. Technol.* **2008**, *42* (10), 3563−3569.
(65) Malvankar, N. S.; Vargas, M.; Nevin, K. P.; Franks, A. E.; Leang, C.; Kim, B. C.; Inoue, K.; Mester, T.; Covalla, S. F.; Johnson, J. P.; et al. Tunable Metallic-like Conductivity in Microbial Nanowire Networks. *Nat. Nanotechnol.* **2011**, *6*, 573−579.
(66) Yang, Z.; Sun, T.; Kleindienst, S.; Straub, D.; Kretzschmar, R.; Angenent, L. T.; Kappler, A. A Coupled Function of Biochar as Geobattery and Geoconductor Leads to Stimulation of Microbial Fe(III) Reduction and Methanogenesis in a Paddy Soil Enrichment Culture. *Soil Biol. Biochem.* **2021**, *163*, 108446.
(67) Zhang, X.; Xia, J.; Pu, J.; Cai, C.; Tyson, G. W.; Yuan, Z.; Hu, S. Biochar-Mediated Anaerobic Oxidation of Methane. *Environ. Sci. Technol.* **2019**, *53* (12), 6660−6668.
(68) Case, S. D. C.; McNamara, N. P.; Reay, D. S.; Stott, A. W.; Grant, H. K.; Whitaker, J. Biochar Suppresses N2O Emissions While Maintaining N Availability in a Sandy Loam Soil. *Soil Biol. Biochem.* **2015**, *81*, 178−185.
(69) Liao, J.; Hu, A.; Zhao, Z.; Liu, X.; Jiang, C.; Zhang, Z. Biochar with Large Specific Surface Area Recruits N_2O-Reducing Microbes and Mitigate N2O Emission. *Soil Biol. Biochem.* **2021**, *156*, 108212.

https://doi.org/10.1021/acs.est.4c14024
Environ. Sci. Technol. 2025, 59, 9576−9586